Thermal annealing as an easy tool for the controlled arrangement of gold nanoparticles in block-copolymer thin films

2013 Nanotechnology 24 255304

(http://iopscience.iop.org/0957-4484/24/25/255304)

Nanotechnology **24** (2013) 255304 (8pp) doi:10.1088/0957-4484/24/25/255304

Thermal annealing as an easy tool for the controlled arrangement of gold nanoparticles in block-copolymer thin films

Ana Ledo-Suárez[1], Cristina Elena Hoppe[2], Massimo Lazzari[1], M Arturo Lopez Quintela[3] and Ileana Alicia Zucchi[2]

[1] Centre for Research in Biological Chemistry and Molecular Materials (CIQUS), c Jenaro de la Fuente—Campus Vida, University of Santiago de Compostela (USC), E-15782 Santiago de Compostela, Spain
[2] Institute of Materials Science and Technology (INTEMA), University of Mar del Plata and National Research Council (CONICET), J B Justo 4302, 7600 Mar del Plata, Argentina
[3] Departamento of Physical Chemistry, Faculty of Chemistry, Campus Vida, University of Santiago de Compostela (USC), E-15782 Santiago de Compostela, Spain

E-mail: massimo.lazzari@usc.es and ileanazu@yahoo.com.ar

Received 19 February 2013, in final form 7 May 2013
Published 30 May 2013
Online at stacks.iop.org/Nano/24/255304

Abstract
Thermal annealing was used for the bottom-up fabrication of morphologically controlled gold–block-copolymer (Au–BC) nanocomposites. Three different blends formed by polystyrene (PS) homopolymer and PS-coated gold nanoparticles (PSSH@Au) were used as modifiers of asymmetric polystyrene-*b*-polymethylmethacrylate (PS-*b*-PMMA): PS_{26}/PS_{26}SH@Au, PS_{75}/PS_{75}SH@Au and PS_{167}/PS_{167}SH@Au (where the subscripts refer to the number of styrene monomeric units).

The results indicated that all three blends used as modifiers (PS_n/PS_nSH@Au) were successfully located in the PS phase during thermally induced BC self-assembly for a composition range from 5 to 43 wt% without macro-phase separation. The PS_nSH@Au moiety experienced molecular desorption, nanocrystal core coalescence and partial molecular re-encapsulation processes during thermal annealing, leading to sphere-like gold NPs with a larger average size (without exceeding an interdomain distance). Ligand chain length regulated the degree of coalescence and re-encapsulation, defining ultimate core size. Furthermore, proper combination of chain length and composition enabled tuning of NP partitioning and arrangement on different length scales through thermally activated cooperative assembly processes. These results have not only significant impact for establishing thermal processing as a useful tool for the precise control of NP size and distribution, but also much broader implications for many nanoparticle-based technologies.

(Some figures may appear in colour only in the online journal)

1. Introduction

Metal nanoparticles (NPs) possess unique, often size-dependent, properties associated with magnetic, photonic, chemical, catalytic and electrical behavior, which are different from the properties in their respective bulk materials [1, 2]. Although the synthesis of such small structures is now relatively easy, their assembly in an ordered fashion onto opportune substrates still remains a challenge, and also has the practical importance of permitting the fine tuning of the NP

properties [3, 4]. Although efforts have been made to decrease the patterning size using standard semiconductor lithography technology [5], fabricating nanostructured materials by bottom-up methods using self-assembling systems has been particularly recognized as an elegant and powerful approach due to its efficiency and high throughput [6, 7]. Among such systems, block-copolymer (BC) templates represent one of the most powerful and exciting self-assembled systems because of the variety of morphologies available, and because their length scale and periodicity can easily be tailored [8–10].

Several experimental methods have been developed for incorporating metal NPs into BC nanostructures. These can be divided into two approaches. The first approach involves the *in situ* synthesis of NPs within BC structures. The synthesis is typically achieved by loading pre-formed BC domains with metal precursors that are subsequently thermally reduced [10–12], although the metallic precursor can also be sequestered in the polymer prior to phase segregation (eventually even by covalent attachment to one of the blocks) [13–16]. However, precise control of the size distribution and shape of NPs within the periodic structure of the BC is difficult. The second approach, recently proposed as a way to avoid some of the drawbacks of the method described above, uses cooperative self-organization of pre-formed NPs and BCs [17, 18]. In this case, the spatial distribution of pre-formed NPs in the microphase-separated morphologies is controlled by selecting opportune polymeric ligands. The main role of such polymeric ligands is to stabilize and control NP formation during synthesis, allowing the initial small size to be maintained by preventing coagulation. At the same time, by tuning their chemical nature in order to favor the selective interaction with one of the blocks of a BC or providing a 'neutral' polymer surface to the nanoparticle, these ligands can orient the location of NPs within the BC template [19, 20]. However, the use of these kinds of polymer-capped NP normally involves time-consuming purification steps to eliminate the excess of free ligand used during the functionalization process.

The main objective of this work is to find a simple, versatile and precise procedure to arrange gold NPs on a BC that could be potentially useful for technological applications. With this objective in mind, we selected thermal processing as the promoter of BC self-assembly and used PS-coated NPs (PSSH@Au), partially purified from excess of free ligand, as the modifier of the system. This implies that the real modifier of the BC is the PS/PSSH@Au blend as obtained from the NP synthetic route. Use of thermal processing has the advantage of avoiding the inconveniences associated with solvent annealing, such as long annealing times and strict control of solvent evaporation rate, solvent selectivity and other environmental conditions, including dewetting phenomena [15].

The proposed approach also takes advantage of the synergic effect that thermal annealing is expected to have on NP/BC blends. In systems prepared with small NPs (<4 nm) coated by a ligand affine with one of the BC blocks, thermal annealing should promote the BC self-assembly, induce preferential location of NPs in one of the phases by softening the material (and allowing the mobility of NPs) and, at the same time, increase NP size and monodispersity by thermal ripening [21, 22]. Hence, we analyzed the viability of simultaneously achieving controlled size growth of NPs and BC assembly by thermal processing. The selected BC was PS-*b*-PMMA, since good-reproducible morphologies have been previously obtained using thermal annealing [23, 24]. We have studied the effect of the addition of different amounts of PSSH/PS@Au, different ligand chain lengths and film thickness on BC morphologies, stability against macro-phase separation and the ordering of NPs.

Table 1. Number average molecular weight, polydispersity index and SH terminal functionalization grade of PS ligands.

Polymer	M_n (g mol^{-1})[a]	M_w/M_n[b]	% SH[c]
$PS_{26}SH$	2 800	1.12	78
$PS_{75}SH$	7 900	1.11	66
$PS_{167}SH$	17 500	1.18	21

[a] Number average molecular weight (M_n) based on ^{1}H NMR measurements.

[b] Polydispersity index obtained by size exclusion chromatography using PS standards.

[c] SH terminal functionalization grade estimated from the integration of ^{1}H NMR signals.

Table 2. Characterization of gold nanoparticles coated by PS chains.

	Particle core diameter (nm)[a]	Particle diameter (core + shell, nm)[b]
$PS_{26}SH@Au$	1.8 ± 0.2	6.6
$PS_{75}SH@Au$	2.7 ± 0.4	11.7
$PS_{167}SH@Au$	3.4 ± 0.6	15.4

[a] Estimated from TEM imaging of at least 200 particles.

[b] Measured by dynamic light scattering (DLS).

2. Experimental section

2.1. Synthesis of $PS_nSH@Au$ NPs

$PS_nSH@Au$ NPs were synthesized by chemical reduction of hydrogen tetrachloroaurate trihydrate in the presence of thiol-functionalized polystyrenes (PS_nSH) of different molecular weights. Monodisperse samples of PS were synthesized by ATRP (see table 1). A subsequent post-treatment process with thiodimethylformamide as sulfur precursor produced polymer chains bearing thiol end groups [48]. Three different kinds of NP were used in this work: $PS_{26}SH@Au$, $PS_{75}SH@Au$ and $PS_{167}SH@Au$, where the subscript refers to the number of styrene monomeric units (M_n = 2800, 7900 and 17 500, respectively). The resulting core diameters were in the range of 1.5–3.5 nm as determined by transmission electron microscopy (TEM) (see table 2). These NPs were prepared avoiding the steps concerning elimination of unbonded PS ligands. Consequently, the modifier employed for the modification of the BC is the mixture $PS_n/PS_nSH@Au$, where the amount of gold in the mixture is about 2 wt% as calculated by TGA.

2.2. Substrate preparation

Silicon pieces (1 × 1 cm^2) were cleaned with fresh piranha solution (1/3 v/v mixture of 30% H_2O_2 and 98% H_2SO_4) at 80 °C for 60 min in order to eliminate any residual organic trace. The pieces were then rinsed in water, cleaned with isopropanol for 15 min in ultrasonic bath and finally dried under vigorous N_2 flow.

2.3. Thin film deposition

Commercial asymmetric PS-*b*-PMMA, with total molecular weight $M_n = 67\,100$ and PDI = 1.09, was purchased from Polymer Source and used without further purification. The volume fraction of PMMA block was 0.29. This BC self-assembled in hexagonal arrangements of ≈18 nm diameter cylindrical PMMA domains (center-to-center spacing or natural domain period $L_0 \approx 36$ nm) in a matrix of PS. Toluene solutions of the BC (1, 3 or 5 wt%) were combined with PS_n/PS_nSH@Au to result in 5–47 wt% final compositions of the modifier. Thin films were obtained by spin coating these solutions at 3000 rpm for 60 s onto previously cleaned Si wafers. Samples with film thicknesses of about 30, 100 and 500 nm were obtained. To promote self-assembly of the BC, the films were heated at 190 °C for 1 h.

2.4. Characterization

The morphology of the polymeric films after thermal treatment was characterized by scanning electron microscopy (SEM, Zeiss Supra 40 with a field emission source or Zeiss FE SEM UltraPlus) operated at an accelerated voltage of 1 keV and using a secondary-electron detector (InLens).

Au–BC nanocomposites were examined by transmission electron microscopy (TEM). A droplet of the solution was evaporated onto a carbon-coated copper mesh grid and analyzed using a Philips CM-12 microscope at an accelerating voltage of 100 kV. Plan-view images were obtained without RuO_4 staining because electron irradiation induced thinning of the PMMA block, producing sufficient contrast for direct imaging [25].

The size and monodispersity of polystyrene-coated gold nanoparticle dispersions were assessed by dynamic light scattering (DLS). Measurements were made with Zetasizer Nano ZS (Malvern UK) equipped with a 4 mW HeNe laser. The analysis was performed with 1 cm optical path cell and each sample was analyzed three times.

Molecular characterization of polystyrene ligands was performed before using them as coating agents. The polydispersity index was estimated by size exclusion chromatography (SEC) using a modular chromatographic system composed by a Waters M-45 pump, a Rheodyne 7010 injection valve, an injection loop and an ERMA 7510 differential refractometer as a detector. Separation was achieved using a four PL-Gel 5 mm (Polymer Labs) columns in series with nominal porosity of the individual columns 500, 103, 104 and 105, respectively. Sample solutions of 0.2% (w/v) concentration were prepared in THF, used also as the eluent (1 ml min^{-1}), and 200 μl injected into the analysis.

^{1}H NMR spectra were recorded in $CDCl_3$ on a Bruker DRX-500 MHz spectrometer to follow the conversion of the end-functionalized moiety into the thiol group.

Thermal gravimetric analysis (TGA) was carried out with a Q5000 IR thermobalance (TA Instruments), with a scanning rate of 20 °C min^{-1}, under a nitrogen atmosphere.

3. Results and discussion

3.1. BC thin film morphology

In order to define the parallel morphology window of the selected PMMA cylinder forming PS-*b*-PMMA, we prepared films of different thickness onto piranha-cleaned silicon, a substrate that is preferentially wetted by the PMMA block [26]. Films with thicknesses of the order of 30 and 100 nm, i.e. dimensions comparable with the BC ordering dimension L_0 and corresponding to a few lattice spacings, respectively, and a much thicker 500 nm film, were prepared and considered as representative to elucidate the influence of film confinement and thermal annealing on the surface pattern formation. Due to the recent publication of more exhaustive studies on this topic [27, 28], such results are herewith discussed mainly to offer the basis for a better understanding of the effect of the PSSH@Au NP addition to PS-*b*-PMMAs. As example, SEM micrographs of spin-coated PS-*b*-PMMA thin films with variable thickness after 1 h annealing at 190 °C are shown in figure 1.

Samples could be clearly analyzed without removing PMMA since the microscope's electron beam damages and partially removes PMMA domains, generating enough contrast in the images [29] (darker gray regions correspond to PMMA and bright ones to PS). A relatively high annealing temperature (190 °C) was selected for promoting the phase separation and formation of large grains, which is very desirable in terms of template generation [30]. At the same time, the high temperature process also allows us to dramatically reduce the annealing time [27, 30], providing an industrially appealing approach for the technological implementation of BC-based lithographic protocols. No significant further evolution of the surface morphology was observed over reasonable timescales, in good agreement with previously reported results [24, 28, 31], suggesting that all the films reached thermodynamic equilibrium structures [32]. As expected, in films 30 and 100 nm thick (figures 1(a) and (b)) parallel cylinders of PMMA included in a PS matrix are clearly formed. This is a consequence of the preferential segregation of the PMMA component to the silicon substrate. Due to the low thickness, the directing effect of the substrate controls the morphology of the whole sample, promoting formation of parallel cylinders all along the thickness of the film. In contrast, an increase of the film thickness to 500 nm caused a perpendicular orientation of PMMA cylinders at the surface of the film (figure 1(c)). This occurs because the strong orientation effect of the silicon surface field dissipates in thicker films. Under these conditions, a morphology

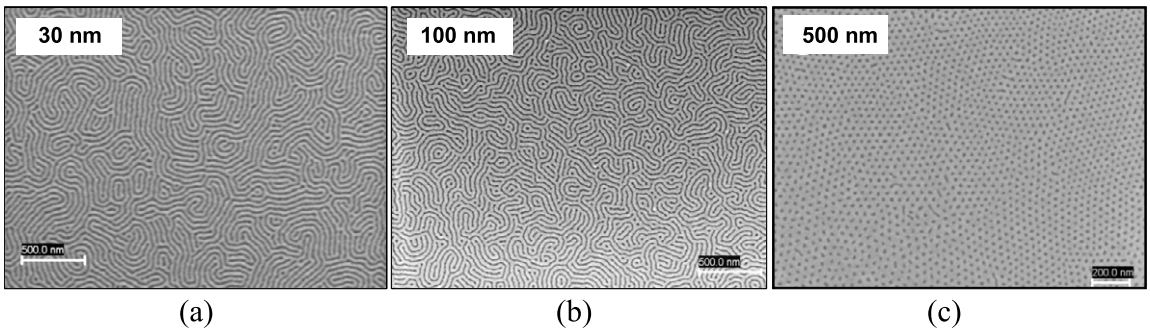

Figure 1. SEM morphology of PS_{461}-*b*-$PMMA_{210}$ thin films.

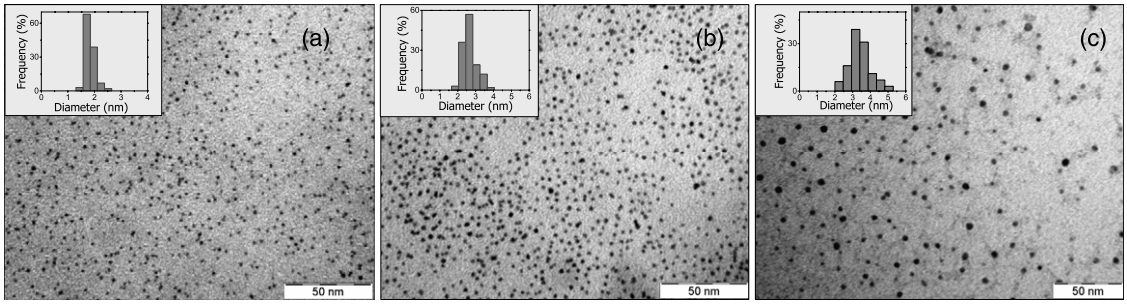

Figure 2. TEM images and size distributions of gold NPs prepared in the presence of (a) $PS_{26}SH$, (b) $PS_{75}SH$ and (c) $PS_{167}SH$. Inset: histograms of gold NP size distributions obtained from TEM images.

characterized by parallel cylinders at the free surface of the film could only be obtained if PS had an especial preference (with respect to PMMA) for the air–polymer surface [33]. However, this is not what occurs in this system, because any preference of the blocks for this interface is almost suppressed by thermal annealing at 190 °C [32, 34].

3.2. Au–BC thin film nanocomposites

Gold NPs with average core diameters in the range 1.8–3.4 nm were prepared by chemical reduction in the presence of PSSH with molecular weight between 2800 and 17 500, figure 2. The PSSH@Au NPs were used as obtained without any further step of elimination of un-bonded PS chains. Consequently, the modifier employed was a mixture of PS_n/PS_nSH@Au.

Toluene solutions of gold NPs were combined with the asymmetric PS-*b*-PMMA diblock copolymer, having an overall molecular weight of 67 100. Figure 3 shows the morphology obtained by SEM of a thin film approximately 30 nm thick of PS-*b*-PMMA modified with 23 wt% of the blend PS_{75}/PS_{75}SH@Au. As observed for pure PS-*b*-PMMA films, no phase separation was visible after spin casting. White domains, corresponding to the core of gold nanoparticles, can be observed preferentially located in the PS phase. This is because of the nature of the capping: although the interaction between gold nanoparticles and PS is neutral, the interaction between the gold-coated particles and the other block (PMMA) is very unfavorable.

Figure 4 shows representative SEM micrographs of approximately 30 nm thick films of PS-*b*-PMMA modified with 23 and 47 wt% of PS_n/PS_nSH@Au after thermal annealing. The different PS_n/PS_nSH@Au blends could be perfectly dispersed in the BC PS domains up to very high modifier loading (at least up to 47 wt%), indicating that conformational entropy penalty associated with the mixing between the PS block chains and the PS/PS@Au blend is not high enough to induce macro-phase separation. As already reported for other PS-based block copolymers [35], gold cores are preferentially located at or near the center of the PS phase, depending on the length of the PSSH capping. In particular, $PS_{26}SH$@Au NPs are located closer to the PS/PMMA interfaces than those capped with $PS_{75}SH$ (figure 5). It should be pointed out that in the TEM images of figure 5 darker gray regions correspond to PS and bright ones to PMMA (opposite to FESEM images) [25]. Such behavior

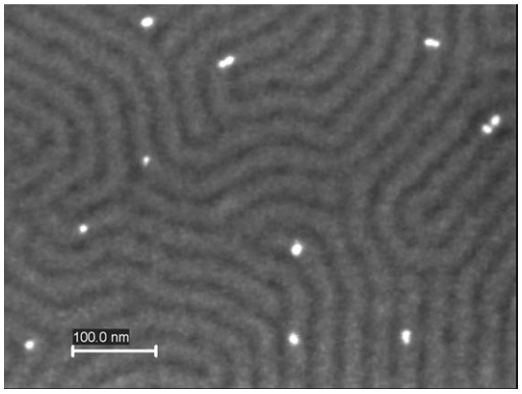

Figure 3. SEM micrograph of a thin film of PS-*b*-PMMA modified with 23 wt% of PS_{75}/PS_{75}SH@Au.

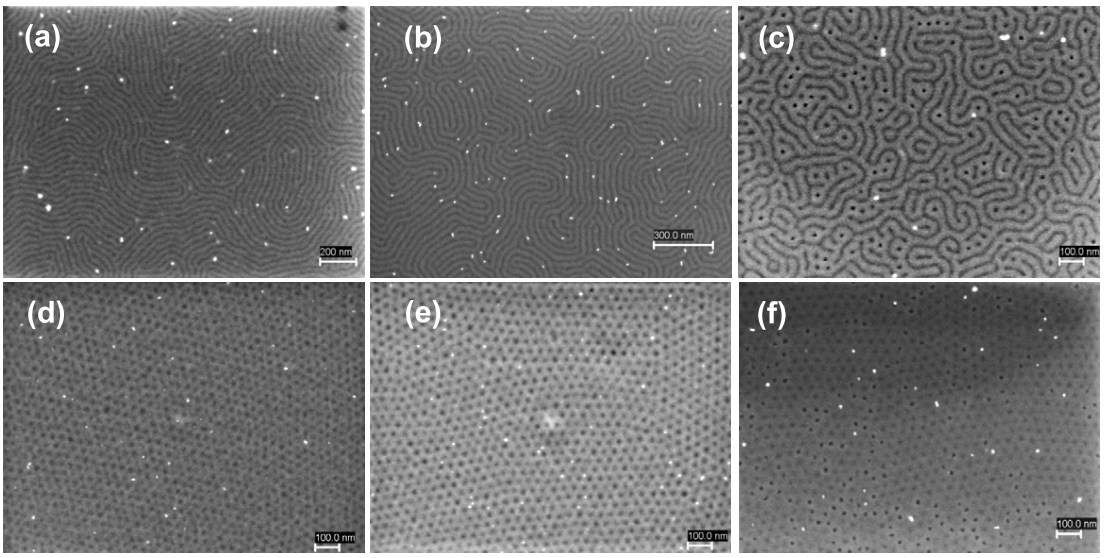

Figure 4. SEM micrographs of 30 nm thick films of PS-*b*-PMMA modified with 23 wt% of PS_{26}/PS_{26}SH@Au (a), PS_{75}/PS_{75}SH@Au (b) and PS_{167}/PS_{167}SH@Au (c) and 47 wt% of PS_{26}/PS_{26}SH@Au (d), PS_{75}/PS_{75}SH@Au (e) and PS_{167}/PS_{167}SH@Au (f).

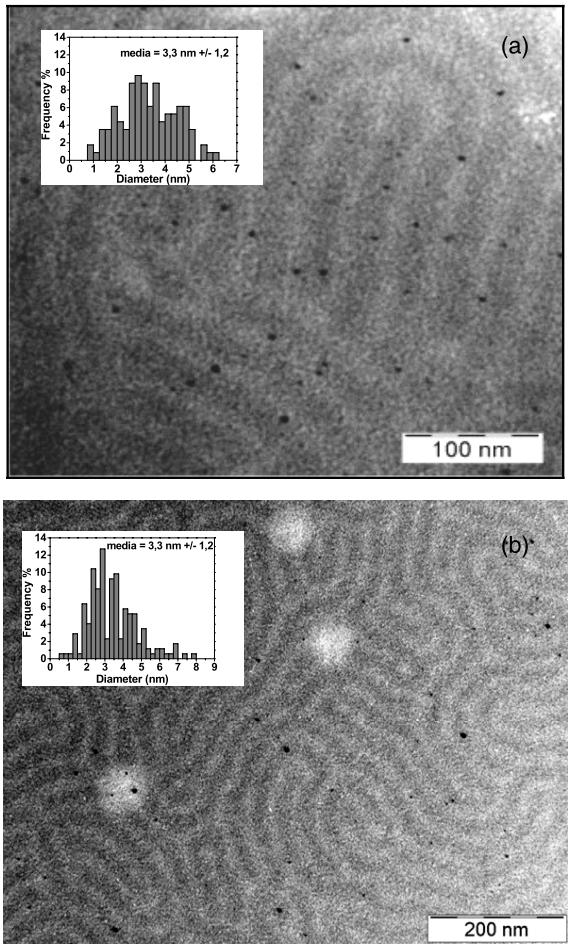

Figure 5. TEM images of PS-*b*-PMMA containing 5 wt% of (a) PS_{26}/PS_{26}SH@Au and (b) PS_{75}/PS_{75}SH@Au. Inset: histograms of gold NP size distributions obtained from TEM images.

may be explained on the basis of residual attractive interaction between the bare gold surface of gold NPs, only partially shielded by the PSSH chains, and the carbonyl group of the PMMA block. As this interaction will be stronger for less protected gold cores (the case of shorter chains), a decrease of the molecular weight of PS would therefore provide for a stronger bonding of NPs to the PS/PMMA interface.

The effect of increasing the amount of modifier on the morphology of the three systems can be seen in figure 4, corresponding to 47 wt% of PS_{26}/PS_{26}SH@Au (d), PS_{75}/PS_{75}SH@Au (e) and PS_{167}/PS_{167}SH@Au (f) in the BC. No evidence of macro-phase separation was observed for any of the formulations, although at the expense of a change from a parallel cylinder to a hexagonally packed dot morphology. These hexagonally packed dots could equally be interpreted as spheres or as ends of cylinders perpendicular to the substrate, because SEM gives images of the top layer of the films. We could speculate that PMMA spheres are a result of an order–order transition from cylinders to spheres induced by the increase in PS volume fraction due to solubilization of the added PS/PS@Au blend. Also, we could speculate that the addition of NPs altered the near surface orientation of PMMA cylinders from parallel to perpendicular. It may be supposed that NP location is affected by the attraction to the negatively charged piranha-treated silicon surface, as already observed for dodecanethiol-coated gold NPs [36]. The attachment of gold colloids onto the otherwise smooth silicon may reduce the attractive potential for the PMMA block to the substrate, diminishing the strength and hence the region of influence of the silicon surface directing field. The self-assembly of PS-*b*-PMMA appears to be affected by such a decrease of orientational effect, leading to perpendicular cylinders in the free surface. Changes in morphology occurring at such high loadings will be the subject of future work, in which GISAXS experiments will be carried out.

An increase in the average core size of NPs was observed, although with different extents, indicating that a coarsening process occurred during the thermally induced self-assembly process. From the histograms of figure 5 we calculated an increase in diameter of 83% in the case

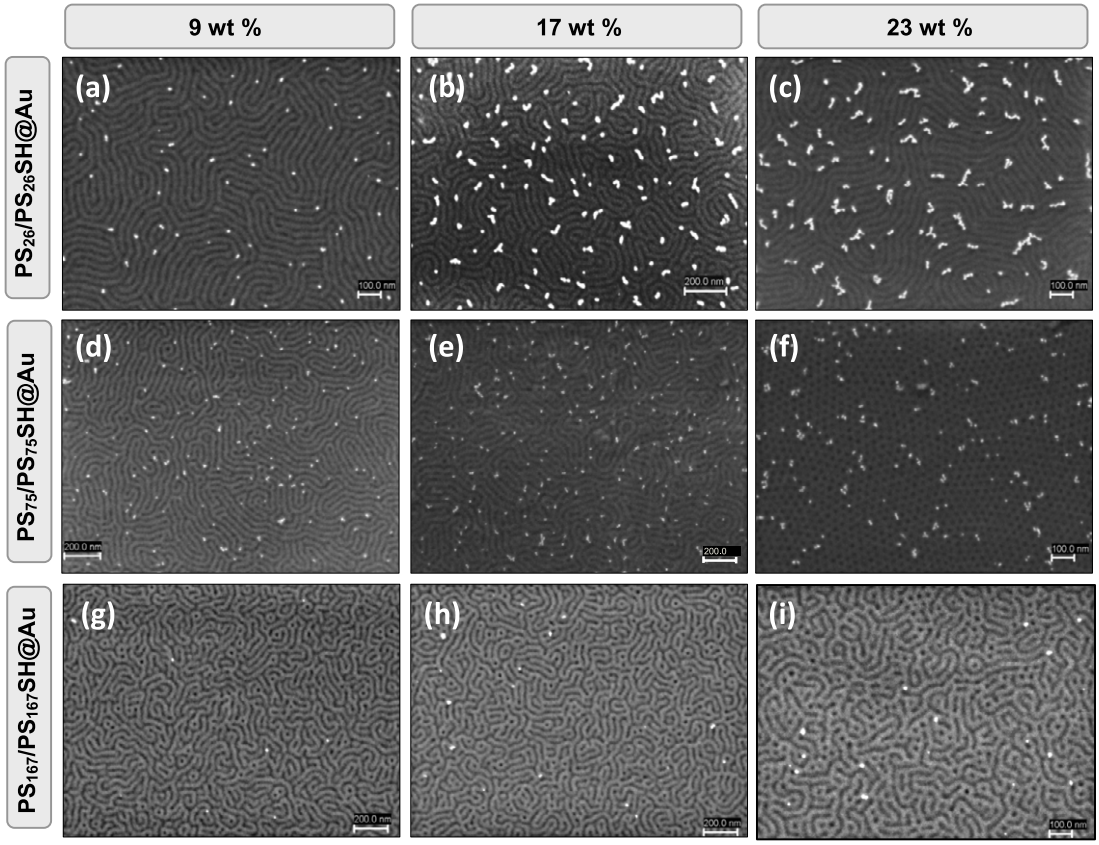

Figure 6. SEM micrographs of 100 nm thick films of PS-*b*-PMMA modified with 9 wt% of PS_{26}/PS_{26}SH@Au (a), PS_{75}/PS_{75}SH@Au (b) and PS_{167}/PS_{167}SH@Au (c), 17 wt% of PS_{26}/PS_{26}SH@Au (d), PS_{75}/PS_{75}SH@Au (e) and PS_{167}/PS_{167}SH@Au (f) and 23 wt% of PS_{26}/PS_{26}SH@Au (g), PS_{75}/PS_{75}SH@Au (h) and PS_{167}/PS_{167}SH@Au (i).

of modification with PS_{26}/PS_{26}SH@Au and 22% in the case of PS_{75}/PS_{75}SH@Au. Coarsening of small gold NPs (2–3 nm) by thermal annealing (in solution and in polymer matrices) has been previously reported as responsible for an increase in size and monodispersity of metal NPs. The main coarsening mechanism operating depends on several variables (temperature, nature and stability of the NP coating, viscosity of the matrix etc). In general, particle migration and coalescence requires a mobile environment and high temperatures, whereas atomic diffusion (associated with the Ostwald ripening mechanism) can occur even in solid embedding media. Nevertheless, combination of both types of mechanism (coalescence and Ostwald ripening) can occur depending on conditions, giving rise to variable final NP morphologies [37–41]. Coalescence of organic modified embedded gold nanocrystals at elevated temperatures has been attributed to the limited temperature stability of the gold–ligand bond and the resulting partial debonding of ligands during thermal annealing [42]. This process has already been reported for alkyl-coated NPs of similar size in solution and in polymeric matrices [37, 43]. Under thermal treatment, coated NPs could suffer a process of ligand desorption followed by the coalescence of the metal core and possible re-adsorption of the polymer onto the newly formed surface. In this case, as the coalescence process is developed inside BC nanodomains, the confinement exerted by the copolymer inhibited the uncontrolled growth of the gold clusters, leading to spherical NPs with an average size smaller than an interdomain distance.

The more pronounced increase in NP size during thermal treatment in the case of modification with the mixture PS_{26}/PS_{26}SH@Au is probably a consequence of the lower protection efficiency associated with shorter polymer ligands. Shell desorption, core coalescence and growth, and shell re-adsorption processes in the thermally activated size evolution of gold NPs are dependent on ligand chain length. The desorption rate is related to the energy barrier required to break the gold–sulfur bond as well as the cohesive van der Waals forces between styrene groups on adjacent styrenethiolates. At thermally enhanced rates of ligand exchange, the shell composition could change and the coalescence of smaller particles into larger particles occurs. The difference in the chain length thus could regulate the degree of coalescence and re-encapsulation and ultimately results in equilibrium core size differences.

In addition, it is worth drawing attention to the location of NPs at the surface or inside the film, as may be appreciated by comparing films with different thicknesses. Figure 6 shows SEM images of films 100 nm thick containing different amounts of PS_n/PS_nSH@Au. As SEM images the top layer of the films, the higher concentration of NPs in the surface (compared to the thinner films of figure 4) seems to indicate an extensive migration of NPs to the free surface. Gold NPs migrate to the surface but remain within the PS microdomains.

Table 3. Number of NPs/μ^2 that reside in the surface of films modified with 23 wt% of $PS_n/PS_nSH@Au$ obtained from SEM images.

	Number of NPs/μ^2		
Thickness	$PS_{26}/PS_{26}SH@Au$	$PS_{75}/PS_{75}SH@Au$	$PS_{167}/PS_{167}SH@Au$
30 nm	21	53	8
100 nm	159	187	10
Increment (%)	660	250	25

This tendency to segregate to the free surface has been previously observed [44–46] and is attributed to surface tension lowering [47]. The other condition that allows NPs to diffuse through the sample toward the free surface is that NPs are dispersed in a continuous phase (the PS matrix); in contrast, they should pay the penalty associated with crossing through an incompatible phase.

Partitioning caused by NP surface migration has the advantage of enhancing the effect of very small concentrations of NPs by accumulating them at the interface. However, as can be clearly appreciated in figure 6 and quantified in table 3, the migration process was determined by the length of the ligand and its interaction with the host polymer. Long, compatible chains will be more effective in inhibiting NP aggregation and migration to the surface than shorter or incompatible coatings. In films modified with 23 wt% of $PS_{167}/PS_{167}SH@Au$ (the longest ligand chain of the three under study), only 25% more NPs were seen when the thickness was increased from 30 to 100 nm (see also figures 4(c) and 6(i)) compared to 660% and 250% increases when using $PS_{26}/PS_{26}SH@Au$ and $PS_{75}/PS_{75}SH@Au$ respectively (see table 3). The high tendency of NPs to reduce surface tension by migrating to the free surface is inhibited by long ligand chains that make NP diffusion through the sample difficult.

The process of migration to the free surface (more appreciable in samples modified with $PS_{26}/PS_{26}SH@Au$ and $PS_{75}/PS_{75}SH@Au$ blends of figure 6) is accompanied by aggregation of NPs in an ordered fashion. A preferential head to tail arrangement is selectively promoted, leading to the formation of gold clusters distributed in the PS phase of the BC film. The rather narrow width of aggregates along with their exclusive location within the PS domains suggests that clustering of particles occurs after the formation of the copolymer microstructure. In this case, the observed average aggregate size is expected to be a consequence of the spatial constraints imposed by the adjacent PMMA domains, chain packing requirements for accommodation of the particle aggregates, and the dynamics of particles and polymer chains during the annealing process.

Hence, different morphologies between two limit cases can be found. For long ligand chain lengths, compatibility with the host polymer is favored and migration to the surface is inhibited, leading to systems with a homogeneous dispersion of NPs throughout the entire sample. In contrast, for short chains, migration and nanoparticle self-assembly are favored and films characterized by gold clusters of larger NPs distributed in the PS phase are obtained (scheme 1). Moreover, attractive interaction between NPs, associated with less protected metallic cores, leads to a 'controlled coalescence' process that took place inside PS domains of the nanostructured PS-*b*-PMMA.

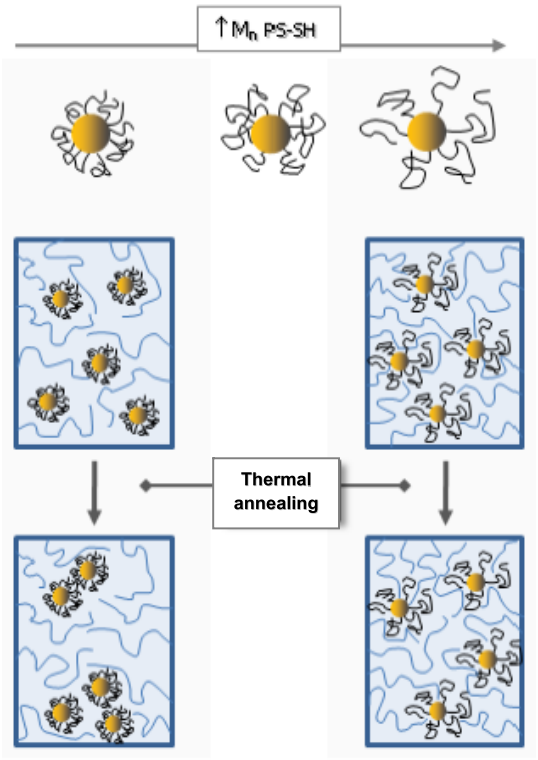

Scheme 1. Evolution of the colloidal system inside PS domains as a function of ligand molecular weight during thermal annealing.

4. Conclusions

We have demonstrated that thermal annealing is an adequate tool for the bottom-up fabrication of morphologically controlled functional nanocomposites. Although well known as a procedure to promote BC nanostructuring, its effect on partitioning, coalescence and aggregation of NPs during thermally induced self-assembly had not been previously analyzed.

Blends of $PS_n/PS_nSH@Au$ were located in the PS phase during thermally induced BC self-assembly without macrophase separation. Concomitant with BC nanostructuration, the $PS_nSH@Au$ moiety experienced molecular desorption, nanocrystal core coalescence and partial molecular re-encapsulation processes during thermal annealing, leading to sphere-like gold NPs with a larger average size without exceeding an interdomain distance (since NPs are dissolved

in the PS phase). However, these processes become weak with the increase in ligand length associated with major protection efficiency of the capping. Thus, ligand chain length regulated the degree of coalescence and re-encapsulation, defining ultimate core size.

Furthermore, through thermally activated cooperative assembly processes, NP partitioning and arrangement on different length scales could be properly tuned by adjusting ligand length and composition. For short ligand chains, migration to the free surface and nanoparticle self-assembly are favored and films characterized by gold clusters randomly distributed in the PS phase are obtained. In contrast, for long ligand chains, compatibility with the host polymer is favored and migration to the surface is inhibited, leading to systems with a homogeneous dispersion of NPs throughout the entire sample.

These results have not only significant impact for the establishment of the thermal processing method as a tool for the precise control of NP size and distribution, but also much broader implications for many nanoparticle-based technologies.

Acknowledgments

The financial support of the University of Mar del Plata, the National Research Council (CONICET) and the National Agency for the Promotion of Science and Technology (ANPCyT) is gratefully acknowledged. ML and ALS are grateful for the financial support by the Xunta de Galicia (PX2010/168-2 and PX2010/152-2), and the FPU grant from the Spanish Ministry of Science and Technology, respectively.

References

[1] Fendler J H (ed) 1998 *Nanoparticles and Nanostructured Films: Preparation, Characterization and Applications* (Weinheim: Wiley–VCH)
[2] Rotello V (ed) 2004 *Nanoparticles: Building Blocks for Nanotechnology* (New York: Kluwer Academic, Plenum)
[3] Zhang H, Han J and Yang B 2010 *Adv. Funct. Mater.* **20** 1533
[4] Balasz A C, Emrick T and Russell T P 2006 *Science* **314** 1107
[5] Pease R F and Chou S Y 2008 *Proc. IEEE* **96** 248
[6] Hamley I W 2009 *Prog. Polym. Sci.* **34** 1161
[7] Whitesides G M, Kriebel J K and Mayers B T 2005 *Nanoscale Assembly* ed W T S Huck (Berlin: Springer) chapter 9
[8] Kamcev J, Germack D S, Nykypanchuk D, Grubbs R B, Nam C-Y and Black C T 2013 *ACS Nano* **7** 339
[9] Ryu D Y, Shin K, Drockenmuller E, Hawker C J and Russell T P 2005 *Science* **308** 236
[10] Darling S B, Yufa N A, Cisse A L, Bader S D and Sibener S J 2005 *Adv. Mater.* **17** 2446
[11] Sohn B H and Seo B H 2001 *Chem. Mater.* **13** 1752
[12] Li J Z, Kamata K and Iyoda T 2008 *Thin Solid Films* **516** 2577
[13] Mendoza C, Pietsch T, Gindy N and Fahmi A 2008 *Adv. Mater.* **20** 1179
[14] Mendoza C, Pietsch T, Gutmann J S, Jehnichen D, Gindy N and Fahmi A 2009 *Macromolecules* **42** 1203
[15] Lee C, Kim S H and Russell T P 2009 *Macromol. Rapid Commun.* **30** 1674
[16] Deshmukh R D, Buxton G A, Clarke N and Composto R J 2007 *Macromolecules* **40** 6316
[17] Abul Kashem M M *et al* 2009 *Macromolecules* **42** 6202
[18] Xu C, Ohno K, Ladmiral V, Milkie D E, Kikkawa J M and Composto R J 2009 *Macromolecules* **42** 1219
[19] Bockstaller M R, Mickiewicz R A and Thomas E L 2005 *Adv. Mater.* **17** 1331
[20] Chiu J J, Kim B J, Kramer E J and Pine D J J 2005 *J. Am. Chem. Soc.* **127** 5036
[21] Fan H Y, Gabaldon J, Brinker C J and Jiang Y B 2006 *Chem. Commun.* **22** 2323
[22] Terzi F, Seeber R, Pigani L, Zanardi C, Pasquali L, Nannarone S, Fabrizio M and Daolio S 2005 *J. Phys. Chem.* B **109** 19397
[23] Zucchi I A, Poliani E and Perego M 2010 *Nanotechnology* **21** 185304 (5pp)
[24] Guarini K W, Black C T and Yeung S H I 2002 *Adv. Mater.* **14** 1290
[25] Thomas E L and Talmon Y 1978 *Polymer* **19** 225
[26] Coulon G, Russell T P, Green P F and Deline V R 1989 *Macromolecules* **22** 2581
[27] Zhang X, Berry B C, Yager K G, Kim S, Jones R L, Satija S, Pickel D L, Douglas J F and Karim A 2008 *ACS Nano* **2** 2331
[28] Han E, Stuen K O, Leolukman M, Liu C-C, Nealey P F and Gopalan P 2009 *Macromolecules* **42** 4896
[29] Huang E, Russell T P, Harrison C, Chaikin P, Register R A, Hawker C J and Mays J 1998 *Macromolecules* **31** 7641
[30] Puglisi R A, La Fata P and Lombardo S 2007 *Appl. Phys. Lett.* **91** 053104
[31] Chen S-C, Kuo S-W, Jeng U-S, Su C-J and Chang F-C 2010 *Macromolecules* **43** 1083
[32] Welander A M, Kang H M, Stuen K O, Solak H H, Muller M, de Pablo J J and Nealey P F 2008 *Macromolecules* **41** 2759
[33] Xu T, Hawker C J and Russell T P 2005 *Macromolecules* **38** 2802
[34] Mansky P, Russell T P, Hawker C J, Mays J, Cook D C and Satija S K 1997 *Phys. Rev. Lett.* **79** 37
[35] Kim B J, Fredrickson G H, Bang J, Hawker C J and Kramer E J 2009 *Macromolecules* **42** 6193
[36] Tzeng S-D, Lin K-J, Hu J-C, Chen L-J and Gwo S 2006 *Adv. Mater.* **18** 1147
[37] Zucchi I A, Hoppe C E, Galante M J, Williams R J J, López-Quintela M A, Matějka L, Slouf M and Pleštil J 2008 *Macromolecules* **41** 4895
[38] Gómez M L, Hoppe C E, Zucchi I A, Williams R J J, Giannotti M I and López-Quintela M A 2009 *Langmuir* **25** 1210
[39] Hostetler M J *et al* 1998 *Langmuir* **14** 17
[40] Alvarez M M, Khoury J T, Schaaff T G, Shafigullin M N, Vezmar I and Whetten R L 1997 *J. Phys. Chem.* B **101** 3706
[41] Jia X, Listak J, Witherspoon V, Kalu E E, Yang X and Bockstaller M R 2010 *Langmuir* **26** 12190
[42] Meli L and Green P F 2008 *ACS Nano* **2** 1305
[43] Maye M M and Zhong C J 2000 *J. Mater. Chem.* **10** 1895
[44] Lin Y *et al* 2005 *Nature* **434** 55
[45] He J B, Tangirala R, Emrick T, Russell T P, Böker A, Li X F and Wang J 2007 *Adv. Mater.* **19** 381
[46] Zou S, Hong R, Emrick T and Walker G C 2007 *Langmuir* **23** 1612
[47] Kim J and Green P 2010 *Macromolecules* **43** 1524
[48] Ledo-Suárez A, Lazzari M and López-Quintela M A in preparation